

Dynamics of amplification in a nanoplasmonic metamaterial

Sebastian Wuestner · Andreas Pusch ·
Joachim M. Hamm · Kosmas L. Tsakmakidis ·
Ortwin Hess

Received: 1 July 2011 / Accepted: 8 December 2011 / Published online: 21 February 2012
© Springer-Verlag 2012

Abstract Plasmonic metamaterials form an exciting new class of engineered media that promise a range of important applications, such as subwavelength focusing, cloaking and slowing/stopping of light. Recently it has been shown that the internal losses due to the natural absorption of metals at optical frequencies can be compensated by gain. Here, we employ a Maxwell–Bloch methodology which allows us to study the dynamics of the coherent plasmon-gain interaction, nonlinear saturation, field enhancement and radiative damping. Using numerical pump-probe experiments on a double-fishnet metamaterial with dye-molecule inclusions we investigate the buildup of the inversion and the formation of the plasmonic modes in the low- Q fishnet cavity. We find that loss compensation occurs in the negative-refractive-index regime and that, due to the loss compensation and the associated sharpening of the resonance, the real part of the refractive index of the metamaterial becomes more negative compared to the passive case. Furthermore, we investigate the behavior of the metamaterial above the lasing threshold, and we identify the occurrence of a far-field lasing burst and gain depletion. Our results provide deep insight into the internal processes that affect the macroscopic properties of active metamaterials. This could guide the development of amplifying and lasing plasmonic nanostructures.

1 Introduction

The conception and development of composite media showing negative electromagnetic parameters [1–3] constitutes

an important recent advance in condensed matter physics, electromagnetics and optics. It has been theoretically shown that negative effective permittivities, permeabilities and refractive indices enable us to cancel the effect of positive constants of standard dielectrics on the propagation or nano-localization of electromagnetic fields. Thereby the characteristic optical parameters can be dramatically reduced or enhanced allowing for regimes beyond the reach of naturally occurring materials. For example, in the field of plasmonics [4] the negative real part of the permittivity ϵ_m of a metal combined with a dielectric response can be used to realize sub-wavelength guiding and manipulation of light signals. Further, high-resolution imaging can be enabled via a negative-refractive-index lens [5, 6] which cancels the phase accumulated in a positive index medium and allows for the restoration of the amplitude of evanescent waves. Other examples in which a ‘negative’ parameter is employed to counteract a ‘positive’ parameter are negative-index-based ‘invisibility’ cloaking [7] and stopping of light in metamaterial and plasmonic waveguides [8, 9].

Unfortunately, in the optical regime the absorption coefficients of passive negative-index metamaterials are high, limiting the practical deployment in the applications outlined above. This is due to the inherent dissipative losses in the metallic inclusions which are necessary to provide a strong electromagnetic response. Since the metamaterial losses exceed typical bulk gain coefficients of active media by more than an order of magnitude a compensation of these losses by gain materials is not straightforward and several studies have been devoted to this problem [10–19]. One of the results of these studies is that the field enhancement due to plasmonic resonances which can substantially (by more than a factor of ten) increase the local fields can also significantly enhance the effective gain coefficients if the gain material is placed into the spots of high electric field strengths [13, 16,

S. Wuestner · A. Pusch · J.M. Hamm · K.L. Tsakmakidis ·
O. Hess (✉)

Blackett Laboratory, Department of Physics, Imperial College
London, South Kensington Campus, London SW7 2AZ, UK
e-mail: o.hess@imperial.ac.uk

17]. It has been shown experimentally in an active double-fishnet metamaterial [15] that this effective gain enhancement makes it possible to fully compensate the dissipative losses in optical metamaterials by using available gain media (in this case a molecular dye). Significant experimental progress has also been achieved in relation to gain-enhanced magnetic metamaterials [11, 18].

Here, we study the gain dynamics of an active double-fishnet metamaterial [20, 21] with geometric parameters given in Fig. 1. The gain model employed in this work is a generic model that can be used to approximate a large variety of different gain materials. Here we adjust the parameters to fit the dye Rhodamine 800 embedded in a dielectric host material [15, 16] with refractive index $n_h = 1.62$. Despite the short lifetime of dye molecules due to photobleaching, limiting their applicability in practical devices, they can be used for proof-of-principle studies and for comprehending and probing the plasmon/gain dynamics in active plasmonic metamaterials. Dyes have the advantage of a comparatively easy integration into metal structures to maximally harness the plasmonic field enhancement whereas integration of crystalline semiconductor gain media (e.g., quantum-wells) is very difficult to achieve.

In order to elucidate the interplay between electromagnetic fields, the free-electron plasma of the metals and the dipolar transitions in the gain medium we directly model the full-vectorial Maxwell's curl equations supplemented by local response models for gain material and metal. This model, outlined in Sect. 2, is able to self-consistently capture the spatial and temporal evolution of plasmonic/light fields naturally emerging from the description of the relevant processes, namely the excitation by pump and probe fields injected from the far field, stimulated emission and absorption in the gain material [16, 22–27], the excitation of (localized) surface plasmons and the decay of the excited modes due to ohmic and radiative damping. In Sect. 3 we analyze the optical properties of the optically pumped double-fishnet in the amplifying regime and show that, by using very high

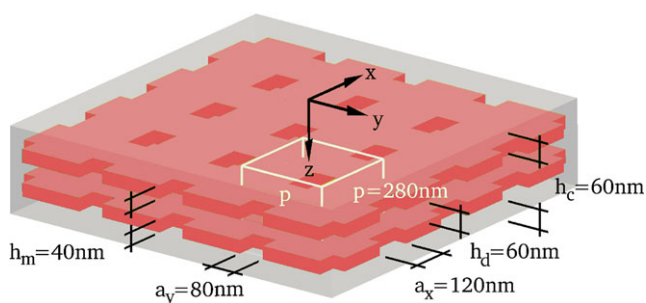


Fig. 1 Illustration of the double-fishnet structure with its associated geometric parameters. A square unit cell with side-length p is highlighted in white. The two perforated silver films are embedded in a dielectric host material (translucent) infiltrated with dye molecules

dye densities, even lasing bursts can be achieved. Finally, in Sect. 4 we draw conclusions from the presented study.

2 Method

Our investigations are based on an auxiliary-differential-equation finite-difference time-domain (ADE-FDTD) method [16, 27, 28] that enables us to not only describe the spatio-temporal evolution of the fields in arbitrary dielectric geometries but also to include the dynamic electronic responses in form of induced polarization currents—even in the nonlinear regime. By directly solving a discretized version of Maxwell's equations, the influence of the plasmonic field enhancements and the spatial inversion pattern of the gain material are self-consistently included in the method.

Plasmonic field enhancement arises from the excitation and propagation of surface plasmons on the interface between the free-electron plasma of a metal and the (bound) electronic structure in a dielectric. The standard model for the electrodynamic response of a free-electron plasma is the Drude response. In this work, this simple but approximate theory is adapted to the measured properties of thin-films of silver in the wavelength range $\lambda = 300\text{--}800$ nm by the inclusion of two Lorentzian resonances [29].

We model the optically pumped gain material as a four-level system with an optical transition for the pump ($0 \leftrightarrow 3$) and for the signal ($1 \leftrightarrow 2$) as shown in Fig. 2. The two dipole transitions are phenomenologically coupled to a four-level system by adding non-radiative carrier relaxation processes $3 \rightarrow 2$ and $1 \rightarrow 0$. Optical transitions between the subsystems ($0, 3$) and ($1, 2$) are considered to be dipole forbidden. We chose the parameters of the model to approximate the experimentally measured characteristics of Rhodamine 800 [30]. Since the measured lineshapes of the absorption and emission lines arise from a combination of homogeneous broadening due to decoherence and inhomogeneous broadening due to a multitude of vibrational states, the Lorentzian lineshapes provide a rough approximation. The gain system is characterized by the following set of parameters (see Fig. 2): The absorption line at $\lambda_{0,a} = 2\pi c/\omega_{0,a} = 680$ nm has a half-width $\Gamma_a = 1/20$ fs $^{-1}$ and a coupling strength $\sigma_a = 1.35 \times 10^{-8}$ C 2 kg $^{-1}$ and the emission line at $\lambda_{0,e} =$

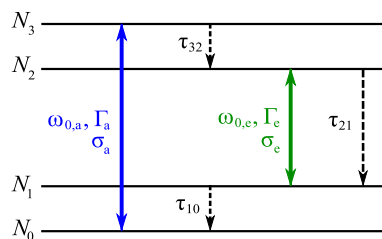


Fig. 2 Sketch of the four-level system and its parameters

710 nm has a half-width $\Gamma_e = 1/20 \text{ fs}^{-1}$ and a coupling strength $\sigma_e = 1.05 \times 10^{-8} \text{ C}^2 \text{ kg}^{-1}$. The dye gain density is $N = \sum_i N_i = 6 \times 10^{18} \text{ cm}^{-3}$ unless otherwise stated. For a detailed description of the gain system see [27] and references therein.

When the dye is pumped on the transition ($0 \leftrightarrow 3$) the four-level model will provide gain at the signal frequency via stimulated emission of the transition ($1 \leftrightarrow 2$). The inversion can be harnessed as gain that is locally coupled into the electromagnetic fields and the local magnitude of the gain depends on the spatial distribution of the electric field and the inversion. Inherently included in the model are also the effects of gain saturation and depletion of the transitions which allows for the observation of nonlinearities such as pump saturation and gain depletion, which manifests itself most strongly in lasing bursts in pump/probe experiments. Although spontaneous emission is not included in this semi-classical model, lasing will be triggered from external excitation if the gain is high enough to overcome dissipative- and radiative losses.

To extract the physical characteristics of the investigated fishnet structure we perform transmission/reflection calculations in which we inject short pulses with planar wavefronts for both the pump and probe fields from the front of the computational domain. The dynamical interaction of these pulses with the spatially resolved features of the double-fishnet metamaterial results in some parts of the pulse being reflected, absorbed and transmitted. By recording time-series of the reflected and transmitted fields at each point of the front- and back-plane of the simulation domain and performing Fourier-transforms, we determine the complex transmission $t(\omega)$ and reflection $r(\omega)$ coefficients. From these we can then calculate the spectral energy fluxes expressed in the transmission $T(\omega) = |t(\omega)|^2$, reflection $R(\omega) = |r(\omega)|^2$ and absorption $A(\omega) = 1 - T(\omega) - R(\omega)$.

We adopt the methodology of [31], which makes an analogy between a metamaterial slab and a dielectric Fabry–Pérot, to extract effective electromagnetic parameters from transmission, reflection and absorption spectra. Retrieving these effective parameters allows us to examine the dispersion and signs of the real and imaginary parts of the homogenized refractive index, permittivity and permeability of the metamaterial. In the presence of gain $\text{Im}(n_{\text{eff}})$ might be negative complicating the retrieval procedure. In this case the validity of the retrieved parameters has to be verified by checking if causality and Kramers–Kronig relations are obeyed [32], a complementary methodology that has been applied successfully in [15, 16].

3 Results and discussion

In the following, we study the plasmon and gain dynamics in the system of Fig. 1, a double-fishnet metamaterial with

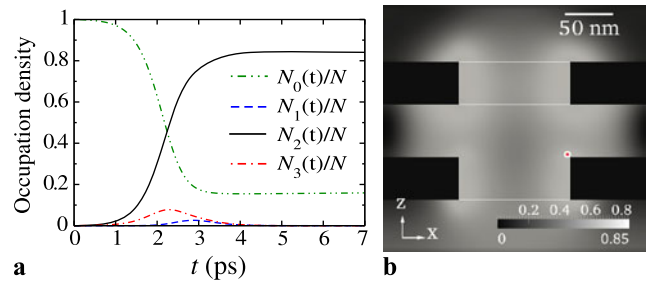


Fig. 3 (a) Time dependence of the occupation densities of the gain medium recorded at a position of high inversion given by a red dot in (b). (b) Snapshot of the occupation inversion after the pump process in a plane inside the double-fishnet unit cell. The white rectangular outlines highlight the positions of the holes and the rectangular black areas are the silver films

embedded gain (here: laser dye). We determine the optical properties of this structure and how these emerge from the properties of its constituents. This is done through numerical pump-probe experiments: A 2 ps pump pulse, polarized along the x -direction, leads to an initial inversion in the gain material and is followed by a short probe pulse, only 12 fs long with the same polarization, that probes the response of the active metamaterial. The delay between pump and probe is 7 ps.

Let us first focus on the pump process. The pump process provides the necessary inversion in order to compensate the metal losses at the probe wavelength. As an example, Fig. 3a shows the characteristic dynamics of the occupation densities for a pump pulse that leads to loss compensation. The dynamic response of the occupation densities is nonlinear, showing strong saturation effects. With initially all molecules in the ground state 0 a large fraction of them is excited by absorption of the pump light. From state 3, the upper absorption state, the electrons relax through non-radiative decay to state 2, the upper emission state, on a time-scale of $\tau_{32} = \tau_{10} = 100 \text{ fs}$. This process leads to a solely transient population being present in state 3 at all times. The lower emission state 1 is temporarily populated due to the coupling of the strong pump pulse to the spectrally broad emission line which leads to stimulated emission. After the pump pulse is switched off and exits the structure (after approximately 4 ps), the transition dynamics slow down and are dominated by non-radiative decay. Accordingly, the very slow decay of N_2 mirrors the relaxation time $\tau_{21} = 500 \text{ ps}$. The long-lived population inversion $\Delta N_e = N_2 - N_1$ of the dye molecules acts back on the propagation of the probe pulse through the structure. This will be studied later.

Figure 3(b) shows the spatial distribution of the inversion after the pump pulse has been switched off with the red dot giving the position where the time-dependent results of Fig. 3(a) were recorded. The occupation inversion in Fig. 3(b) highlights the spatial non-uniformity of the in-

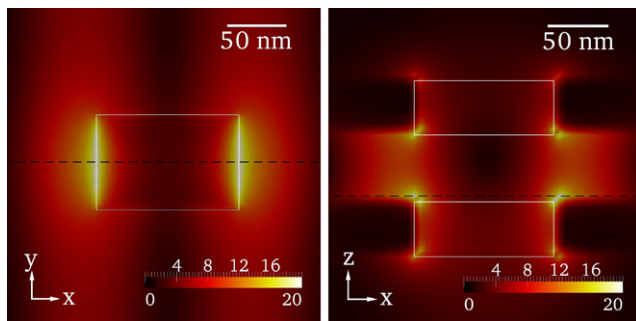


Fig. 4 Electric field enhancement at the probe wavelength in the x - y (left) and the x - z planes (right) of the double-fishnet unit cell. Lighter colors correspond to higher field enhancements. White rectangles outline the holes and the two planes intersect at the black dashed line

version profile where the highest values are located close to the metal. This distribution can be compared to the field enhancement of the pump field, which has generated the inversion. The modal profile at the pump wavelength is similar to the one at the probe wavelength shown in Fig. 4. At the pump wavelength, however, the electric field enhancement reaches maximum values up to 10 only, whereas factors up to 20 are obtained at the probe wavelength. Clearly, higher field enhancements, as seen close to the edges and corners of the metal films, entail higher local inversion of the gain material. At the positions of highest field enhancement, though, this relationship is broken by saturation limiting the maximum inversion. The origin of the high electric field enhancement lies in the excitation of surface plasmons in the resonant double-fishnet structure. These plasmons are supported by and bound to the metal films explaining the mode profile and its field enhancement.

The spatio-temporal evolution of the inversion ΔN_e can be appreciated from the series of consecutive inversion profiles in Fig. 5. While the mode profile at the pump wavelength does not vary much with time (only through a change in the dispersion of the dye), the inversion changes significantly during the pump time. Initially a strong localization, indicative of the field enhancement in Fig. 4, is seen which subsequently spreads outwards into other parts of the dye. This expansion of saturation-limited inversion nonetheless retains the shape of the pump field enhancement, i.e. positions of low field enhancement only show low values of inversion.

After studying the pump process we now turn to the interaction of the inverted gain medium with the plasmonic resonance close to the emission wavelength at $\lambda = 710$ nm. Transmission/reflection measurements of the probe pulse show a transmission maximum at 705 nm and an absorption maximum at 709 nm before the structure is subjected to the pump pulse, see red lines in Fig. 6. After the strong pump pulse has left the structure the transmission peak is enhanced by a factor of 2.5, narrowed to a half-width of approximately 4 nm and shifted to 707.5 nm towards the dye

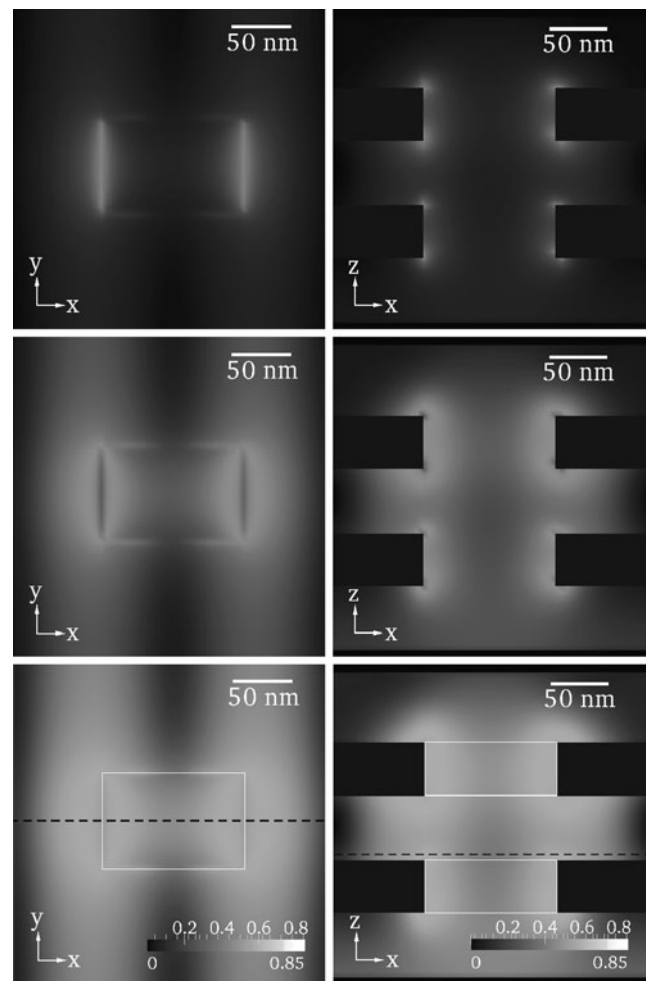


Fig. 5 Snapshots of the occupation inversion ΔN_e during the pump process in two perpendicular planes in a unit cell of the double fishnet. The snapshots are taken (from top to bottom) after 1.36 ps, 2.04 ps and 3.40 ps. The maximum intensity of the pump pulse is reached after approximately 2.9 ps. In the lowest row the white rectangles highlight the position of the holes and the black dashed lines show the intersection of the two planes. The rectangular black areas in the right column are intersections with regions that do not contain gain media (metal films and free space)

emission maximum. The reduction of the half-width is due to the compensation of the metal losses with the resultant half-width coming from radiation losses, i.e. the strong interaction of the plasmonic resonance with the far field. More importantly, the absorption spectrum shows a minimum with negative values in a range of 7 nm around 710 nm. This confirms that the internal dissipative losses are compensated and that the sum of reflection and transmission exceed the input intensity. Nonetheless, the structure is not an amplifier as the transmission does not exceed 1.

The chosen full-time-domain approach also puts us in a position to investigate the dynamic decay of the field energy inside the double-fishnet metamaterial. In [27] we have shown that without inversion the electromagnetic energy de-

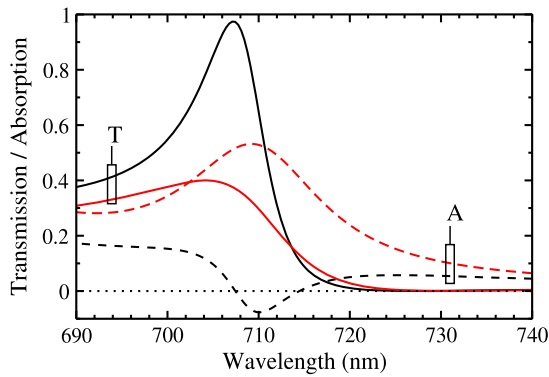


Fig. 6 Transmission T (full lines) and absorption A (dashed lines) before (red lines) and after (black lines) the creating the necessary inversion for loss compensation

increases exponentially with $\tau \approx 14.8$ fs which corresponds to a Q factor $Q = 2\pi\tau/T \approx 40$ (the period is $T \approx 2.37$ fs). Here, the field decay comes from the sum of dissipative and radiative damping. If the metal losses are compensated the Q factor increases to twice its original value ($Q \approx 85$).

In Fig. 6 we have seen that there is a wavelength region where the absorption in the loss-compensated metamaterial becomes negative. Does the same hold for the imaginary part of the effective refractive index $\text{Im}(n_{\text{eff}})$? In order to avoid bianisotropy [33], which would prevent us from discussing these aspects in terms of $\text{Im}(n_{\text{eff}})$, the structure in our computational study is deliberately placed in air instead of assumed to sit on a (thick) substrate (see Fig. 1). First, we extract the effective refractive index, as explained in the methods section, in the case without pumping. The full red line in Fig. 7(a) features a wavelength range between 700 nm and 740 nm where $\text{Re}(n_{\text{eff}}) < 0$. As expected for this purely absorptive case, $\text{Im}(n_{\text{eff}})$ always stays positive. Figure 7(b) shows that the maximum figure of merit $\text{FOM} = -\text{Re}(n_{\text{eff}})/\text{Im}(n_{\text{eff}})$ is close to 2 then. Above loss compensation the effective parameters change quite dramatically. Resonant features are more pronounced and $\text{Im}(n_{\text{eff}})$ now becomes negative around the emission wavelength of the dye at 710 nm. The wavelength range of $\text{Im}(n_{\text{eff}}) < 0$ approximately matches the region where we have seen negative values for the absorption in Fig. 6. More importantly, $\text{Re}(n_{\text{eff}})$ stays negative in this wavelength range and simultaneous negative real and imaginary parts of the refractive index are realized. Figure 7(b) shows that the figure of merit diverges at the positions where $\text{Im}(n_{\text{eff}})$ crosses zero, highlighted by the vertical dotted lines which therefore enclose the region of $\text{Im}(n_{\text{eff}}) < 0$.

In addition to the smoothness of the retrieved parameters, which indicates the correct implementation of the parameter retrieval, a further verification relies on the Kramers–Kronig relations as pointed out in the methods section. The inset in Fig. 7(a) compares the real and imaginary parts of the effective permeability calculated as in [31] (full lines) with

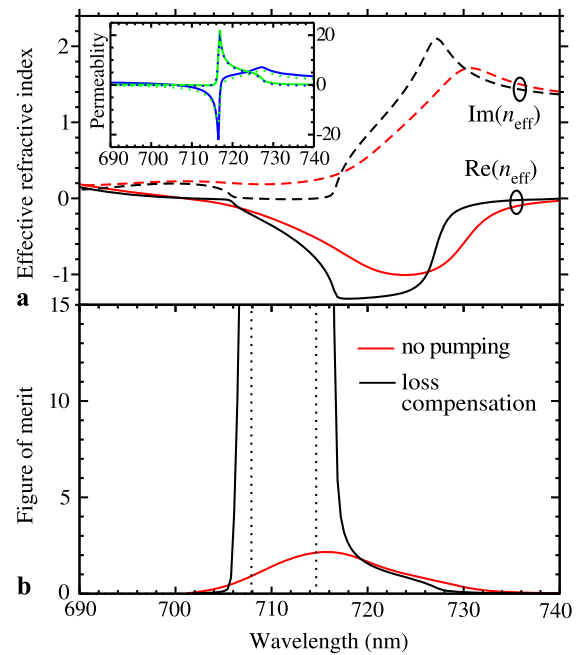


Fig. 7 (a) Real and imaginary parts of the retrieved effective refractive indices without pumping (red line) and above loss compensation (black line). The inset shows the real and imaginary parts of the effective permeability (blue and green line, respectively) and the cross-result of the Kramers–Kronig relation (blue and green dotted lines) for the loss-compensated case. (b) The figures of merit (FOMs) for the effective refractive indices of (a). The vertical dotted lines highlight the wavelength range where the imaginary part of the refractive index is negative above loss compensation

the cross-results of the Kramers–Kronig relations applied to the retrieved permeability (dotted lines). Both the real and imaginary parts are in good agreement which proves that the Kramers–Kronig relations and therefore causality are obeyed.

Next to the aspect of loss compensation, the full-time-domain Maxwell–Bloch theory is inherently capable of describing the nonlinear effects, particularly those that begin to dominate at higher gain values when a transition into the lasing regime can occur (see Fig. 8). As we saw from the Q factor of the loss-compensated metamaterial resonance [27], a significant amount of radiative losses would have to be overcome to achieve lasing. However, increasing the density of dye molecules by a factor of four to $2.4 \times 10^{19} \text{ cm}^{-3}$ the gain can, indeed, overcome radiative as well as dissipative losses. In Fig. 8(a) we show the pulse for $1.2 \times 10^{19} \text{ cm}^{-3}$ (red line) being amplified at the emission wavelength, and, in accordance with experimental results [15], no lasing instability is encountered yet. With a higher dye density of $2.4 \times 10^{19} \text{ cm}^{-3}$ (black line) the lasing threshold can, however, be exceeded leading to a lasing burst and gain depletion, as shown in Fig. 8(b). In the absence of continuous pumping, the gain depletion will cause a breakdown of the

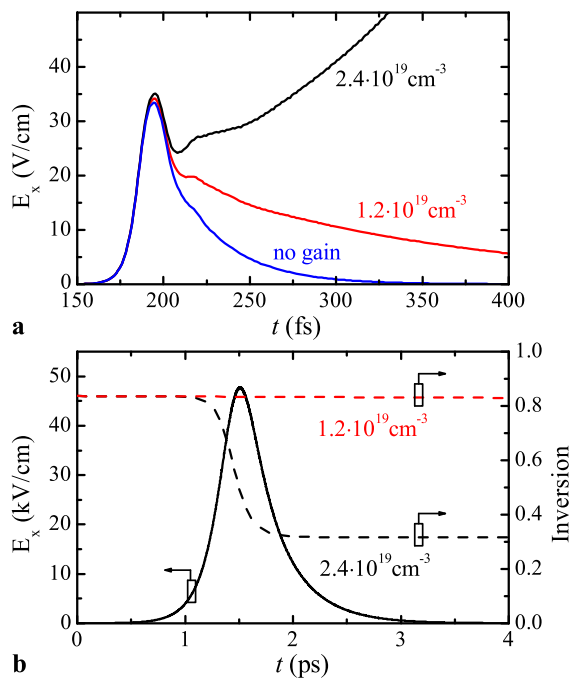


Fig. 8 (a) Envelope of the electric far-field E_x without gain medium (blue line) and for gain densities $N = 1.2 \times 10^{19} \text{ cm}^{-3}$ (red line) and $N = 2.4 \times 10^{19} \text{ cm}^{-3}$ (black line). (b) Left: Envelope of the electric far-field E_x for the gain density $N = 2.4 \times 10^{19} \text{ cm}^{-3}$. Note the change of scale from V/cm in (a) to kV/cm in (b); right: inversion at a position of high field enhancement (black and red dashed lines)

coherent lasing state since no energy is provided to sustain a stable oscillator state with continuous wave output.

4 Conclusion

In summary, we have conducted numerical pump-probe experiments and obtained an insight into the dynamical interplay between gain inversion and (coherent) plasmonic fields that led to full compensation of dissipative losses in the considered double-fishnet metamaterial. The presented spatio-temporal results highlight the importance of having a good overlap of the maximum local gain coefficients with the plasmonic field enhancement in order to enable full loss compensation. Specifically for a double-fishnet metamaterial, the gain material has to be placed in the region between the two silver films. For a strongly pumped configuration, transmission/reflection measurements revealed the presence of a wavelength region where negative absorption coincided with a negative-refractive index. Due to the high radiative outcoupling, lasing instabilities will only occur for dye (gain) densities which are about a factor four higher than what is required for loss compensation, a fact that makes stable amplifier operation possible over a broad regime.

Acknowledgement We gratefully acknowledge financial support provided by the EPSRC, the Royal Academy of Engineering and the Leverhulme Trust.

References

1. N. Engheta, R.W. Ziolkowski, *Electromagnetic Metamaterials: Physics and Engineering Explorations* (Wiley/IEEE Press, New York, 2006)
2. R. Marqués, F. Martín, M. Sorolla, *Metamaterials with Negative Parameters: Theory, Design and Microwave Applications* (Wiley-Interscience, New York, 2008)
3. W. Cai, V. Shalaev, *Optical Metamaterials: Fundamentals and Applications* (Springer, Heidelberg, 2009)
4. S.A. Maier, *Plasmonics: Fundamentals and Applications* (Springer, Heidelberg, 2007)
5. J.B. Pendry, *Phys. Rev. Lett.* **85**, 3966 (2000)
6. N. Fang, H. Lee, C. Sun, X. Zhang, *Science* **308**, 534 (2005)
7. J.B. Pendry, *Nature (London)* **460**, 579 (2009)
8. K.L. Tsakmakidis, A.D. Boardman, O. Hess, *Nature (London)* **450**, 397 (2007)
9. Q. Gan, Z. Fu, Y.J. Ding, F.J. Bartoli, *Phys. Rev. Lett.* **100**, 256803 (2008)
10. M. Wegener, J.L. García-Pomar, C.M. Soukoulis, N. Meinzer, M. Ruther, S. Linden, *Opt. Express* **16**, 19785 (2008)
11. E. Plum, V.A. Fedotov, P. Kuo, D.P. Tsai, N.I. Zheludev, *Opt. Express* **17**, 8548 (2009)
12. A. Fang, T. Koschny, M. Wegener, C.M. Soukoulis, *Phys. Rev. B* **79**, 241104 (2009)
13. Y. Sivan, S. Xiao, U.K. Chettiar, A.V. Kildishev, V.M. Shalaev, *Opt. Express* **17**, 24060 (2009)
14. A. Fang, T. Koschny, C.M. Soukoulis, *J. Opt.* **12**, 024013 (2010)
15. S. Xiao, V.P. Drachev, A.V. Kildishev, X. Ni, U.K. Chettiar, H.-K. Yuan, V.M. Shalaev, *Nature (London)* **466**, 735 (2010)
16. S. Wuestner, A. Pusch, K.L. Tsakmakidis, J.M. Hamm, O. Hess, *Phys. Rev. Lett.* **105**, 127401 (2010)
17. A. Fang, T. Koschny, C.M. Soukoulis, *Phys. Rev. B* **82**, 121102 (2010)
18. N. Meinzer, M. Ruther, S. Linden, C.M. Soukoulis, G. Khitrova, J. Hendrickson, J.D. Olitzky, H.M. Gibbs, M. Wegener, *Opt. Express* **18**, 24140 (2010)
19. A.D. Boardman, V.V. Grimalsky, Y.S. Kivshar, S.V. Koshevaya, M. Lapine, N.M. Litchinitser, V.N. Malnev, M. Noginov, Y.G. Rapoport, V.M. Shalaev, *Laser Photonics Rev.* **5**, 287 (2011)
20. S. Zhang, W. Fan, K.J. Malloy, S. Brueck, N.C. Panoiu, R.M. Osgood, *Opt. Express* **13**, 4922 (2005)
21. S. Zhang, W. Fan, B.K. Minhas, A. Frauenglass, K.J. Malloy, S.R.J. Brueck, *Phys. Rev. Lett.* **94**, 037402 (2005)
22. E. Gehrig, O. Hess, *Spatio-Temporal Dynamics and Quantum Fluctuations in Semiconductor Lasers* (Springer, Heidelberg, 2003). Chap. 7.4
23. A. Klaedtke, J. Hamm, O. Hess, *Lect. Notes Phys.* **642**, 75 (2004)
24. A. Klaedtke, O. Hess, *Opt. Express* **14**, 2744 (2006)
25. K. Böhringer, O. Hess, *Prog. Quantum Electron.* **32**, 159 (2008)
26. K. Böhringer, O. Hess, *Prog. Quantum Electron.* **32**, 247 (2008)
27. S. Wuestner, A. Pusch, K.L. Tsakmakidis, J.M. Hamm, O. Hess, *Philos. Trans. R. Soc. A* **369**, 3525 (2011)
28. A. Taflove, S.C. Hagness, *Computational Electrodynamics: The Finite-Difference Time-Domain Method*, vol. 3 (Artech House, Norwood, 2005)
29. J.A. McMahon, Y.M. Wang, L.J. Sherry, R.P. Van Duyne, L.D. Marks, S.K. Gray, G.C. Schatz, *J. Phys. Chem. C* **113**, 2731 (2009)
30. P. Sperber, W. Spangler, B. Meier, A. Penzkofer, *Opt. Quantum Electron.* **20**, 395 (1988)
31. D.R. Smith, S. Schultz, P. Markoš, C.M. Soukoulis, *Phys. Rev. B* **65**, 195104 (2002)
32. J.J.H. Cook, K.L. Tsakmakidis, O. Hess, *J. Opt. A, Pure Appl. Opt.* **11**, 114026 (2009)
33. C.E. Kriegler, M.S. Rill, S. Linden, M. Wegener, *IEEE J. Sel. Top. Quantum Electron.* **16**, 367 (2010)